# Radiation Pattern Analysis of Mills Cross Array of Patch Antennas for 5G Mobile Handset Applications

**M. J. Martínez Silva, M. S. Ruiz Palacios**

Universidad de Guadalajara, Guadalajara, Jalisco, Blvd. Marcelino García Barragán #1421, C.P. 44430, México, martin.msilva@academicos.udg.mx (Departamento de Electrónica, CUCEI)

***Abstract*— This document presents the analysis of the radiation pattern of Mills cross arrays of patch antennas for a 5G mobile handset in the 28 GHz band. Emphasis is given to determine the radiation coverage in the $z>0$ hemisphere. As a reference to compare the performance of the Mills cross, a square planar array is used. It is found that although square planar array have better performance, the Mills cross can produce directivities up to 16.7 dB with 17 antennas, having total azimuthal coverage up to $\theta=40°$, while it is necessary to use 91 antennas in a square planar array to cover up to $\theta=50°$.**

***Keywords—Mills cross, planar antenna array, 5G antenna.***

## I. INTRODUCTION

The fifth generation (5G) cellular communication system is expected to support more traffic volume, many more devices with diverse service requirements, and provide a better quality of user experience than its predecessor (Groups, 2016). Among other improvements, it has been proposed that 5G will offer user experienced data rate up to 100 Mbps (20 Gbit/s peak) in the downlink direction, and 50 Mbps (10 Gbit/s peak) in the uplink direction (Working Party 5D, 2017). In order to achieve these capabilities, a very wide bandwidth is required, so it has been proposed to use carrier frequencies above 6 GHz, one of the candidates is the 28 GHz band (Recommendation ITU-R, 2015). This solution comes with some drawbacks which must be solved. At this frequency, which is just below the millimeter wave band, the free space propagation produces high path loss (about 17 times or 24.6 dB more loss than for a 1700 MHz LTE system). One way to overcome this phenomenon is to use highly directive antennas. This means that the link will be greatly dependent on the orientation of the antennas in the transmitter and the receiver, something that is not desirable for a mobile communication system. However, it has been proposed to use electronically steerable antenna arrays in the base station or in both, the base station and the handset to solve this problem (Y. Huo, 2017). It is widely known that uniform planar antenna arrays produce pencil shape pattern that can be steerable applying progressive phase signals to the antennas of the array (Balanis, 2005). It is technically feasible to implement such a system using radio frequency integrated circuits (Razavi, 2009). Moreover, massive MIMO techniques have been proposed for 5G to provide simultaneous service to a large number of users (Marzetta, 2015). In (Y. Huo, 2017) the authors propose to use a number of antenna arrays at the user equipment to provide simultaneously high directivity radiation patterns and MIMO capability at 28GHz.

The cost of a miniature electronically steerable planar phase array for a mobile handset will depend on the number of antennas in the array. One scenario is based in beamforming modules (Y. Huo, 2017) that will have the millimeter wave frontend including power amplifiers, low noise amplifiers, besides the control and calibration circuits. If the handset has to be maintained with the lowest cost as possible, it is useful to minimize the number of antennas in the array. In this paper we analyze the radiation pattern properties of a non rectangular planar array called the Mills cross, to be used in a mobile handset for 5G applications.

## II. THE MILLS CROSS

The Mills cross was proposed in (Mills, 1953) as a low cost planar array for radio astronomy capable of producing a narrow pencil receiving beam at meter wavelengths. It consists of two linear antenna arrays located on a plane, perpendicularly oriented one each other, and intercepting at the center, as shown in Fig. 1. By using resourceful coupling and combining networks, as well as switching capability, the signals of the 24+24 dipoles prototype in (Mills, 1953) were processed to produce a 1° pencil beam directed to the zenith.

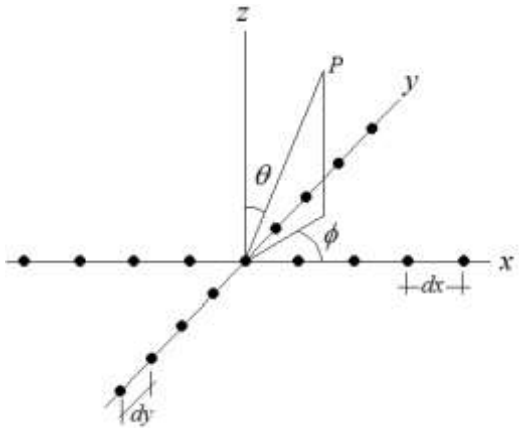


Fig. 1. Mills cross array of 17 elements ($M$=$N$=4).

Additionally to radio astronomy, the Mills cross has been studied and used in a variety of remote sensor areas, including radar (Slattery, 1966), sonar (Degel C., 2014) and seismology (E., 1965). Recent advances have shown that non-uniform

excitation Mills cross can function as a square uniform planar array (H, 2007 ). Moreover, it has been shown that T-shaped arrays can function as the Mills cross (Liang, 2011), (Degel C., 2014).

The array factors of the two arrays of isotropic antennas centered in the origin, as in Fig. 1 are obtained as:

$$A_x = \sum_{m=-M}^{m=+M} I_{xm} e^{jm\left(kd_x \sin\theta\cos\phi+\beta_x\right)} \quad (1)$$

$$A_y = \sum_{n=-N}^{n=+N} I_{yn} e^{jn\left(kd_y \sin\theta\sin\phi+\beta_y\right)} \quad (2)$$

for $0 \le \theta \le \pi$ and $0 \le \phi \le 2\pi$ . In (1) and (2), $k$ is the wavenumber of the propagating wave, $2M+1$ and $2N+1$ are the number of elements of the arrays on each axis. $I_{xm}$ and $I_{yn}$ are the amplitude of excitation of the $n$'th and $m$'th element, $\beta_x$ and $\beta_y$ are the progressive phase of the excitation between the elements, in the respective array. The element $m=0$ and $n=0$ refer to the same center element of the cross, which is common to both arrays. If we suppose a radiating array, and that the electric field produced by one element of the array is $\mathbf{E}_e$ , the total field can be written as:

$$\mathbf{E}_T = \mathbf{E}_e A_x + \mathbf{E}_e A_y = \mathbf{E}_e \left(A_x + A_y\right)$$

Thus, the array factor of the Mills cross is

$$A = A_x + A_y \quad (3)$$

Comparing this array factor with the array factor of a rectangular array (Balanis, 2005)

$$A = A_x A_y$$

we find that in a rectangular array, the array factor results from the multiplication of the array factors of the arrays along each axis, while in the cross array, it corresponds to the addition of the array factors. It is useful to note that for a cross array, the total number of antennas is $2\left(M+N\right)+1$ , while, for a rectangular planar array, the total number of antennas is $\left(2M+1\right)\left(2N+1\right)$.

It is of interest to explore the radiation of the Mills cross when symmetry is used. If we use the same number of elements in both arrays and if the amplitudes of excitation of the antennas are symmetric respect to the center, that is, $I_m = I_{-m}$ , and also, if the separation of the elements are the same in both arrays ( $d_x = d_y = d$ ) it is possible to write the array factor as

$$A = 2I_0 + 2\sum_{m=1}^{M} I_m \left[\cos\left(m\psi_x\right) + \cos\left(m\psi_y\right)\right] \quad (4)$$

where

$$\psi_x = kd\sin\theta\cos\phi + \beta_x \quad (5a)$$

$$\psi_y = kd\sin\theta\sin\phi + \beta_y \quad (5b)$$

As an example, Fig. 2a shows the array factor of a symmetric Mills cross with $N=4$ ( 17 elements), half wavelength separation, side lobe ratio of 20 dB Dolph-Tschebysheff excitation (Balanis, 2005) (normalized amplitudes: $I_0 = 0.53$ , $I_1 = 1$ , $I_2 = 0.85$ , $I_3 = 0.65$ and $I_4 = 0.63$ ) and progressive phases of $\beta_x = 90°$ and $\beta_y = -90°$ . For comparison purposes, Fig. 2b shows the array factor of a $9\times9$ square planar array (81 elements) with the same separation, amplitude and phase distribution. It is clear that the square planar array produces two well laid main lobes, with reduced side lobes due to the multiplication of array factor in both axes. Even though the cross array produces larger side lobes, it has considerably less elements.

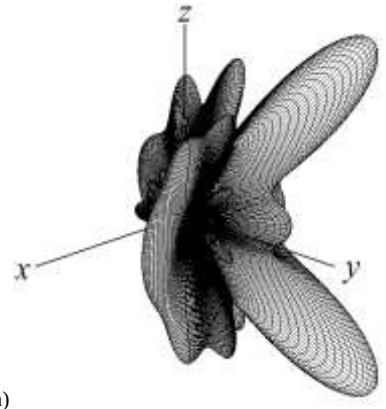


a)

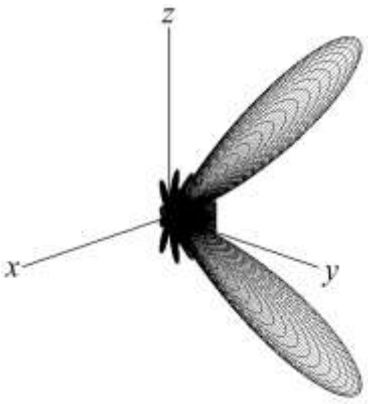


b)

Fig. 2. Array factor produced by: a) 17 elements Mills cross; b) 81 elements square planar array.

## III. PATCH ANTENNA DESIGN

In order to consider the complete radiation pattern of the array, it is necessary to include the antenna to be used as the element of the array. In this case, it has been chosen a rectangular patch antenna because it has a radiation pattern which is directive in accordance with the expected radiation pattern of the array. The design procedure should include the selection of a dielectric substrate with appropriate permittivity and low loss in the low millimeter wave band. In this case, it was selected the Rogers RO4003C hydrocarbon ceramic laminate with a relative permittivity of 3.38, loss tangent of 0.0027, and recommended frequency up to 50 GHz. Selecting a substrate height of 0.305 mm, following the design procedure from (Balanis, 2005) for the calculation of a rectangular patch

antenna for 28 GHz, and after simulation and optimization it is found that the patch size should be $W = 2.79$ mm , $L = 2.39$ mm and the feed point from the edge of the patch $y_0 = 0.5$ mm . The simulated normalized electric field pattern is shown in Fig. 3a, while input reflection coefficient in dB is shown in Fig. 3b, where it is clear that input impedance bandwidth is more than 1 GHz.

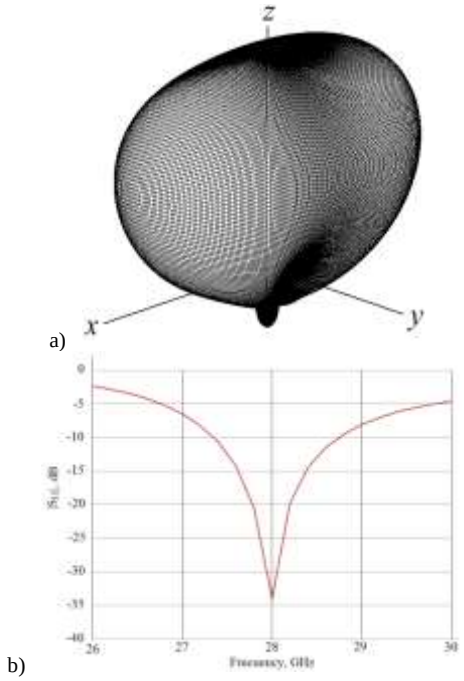


Fig. 3. Patch antenna: a) Normalized field 3D pattern; b) Input reflection coefficient (50Ω).

## IV. RADIATION PATTERN ANALYSIS

In order to analyze the radiation pattern produced by the Mills cross of patch antennas, we will define the parameters of interest and establish a reference for comparison. One of the more reasonable references to use as a model to compare with is the square planar array when it has the same number of antennas in its axes than that used in the Mills cross. Although it is useful to calculate and compare the array factor of the arrays only, it is more realistic to evaluate the properties of the total radiation pattern including the antenna element because this will lead to the knowledge of the covering area of both arrays, at least for one practical antenna. According to antenna array theory, we can use the principle of pattern multiplication for the calculation of total radiation pattern. In general, it is expected to produce a directive radiation pattern with the main lobe electronically steered to cover the $z > 0$ hemisphere as much as possible, with a narrow beamwidth and high directivity. The parameters of interest in this analysis are: The direction of main lobe, beamwidth in two perpendicular axes, and the directivity.

As an example, Fig. 4a and Fig. 4b shows the total field pattern when the array factors shown in Fig. 2a and Fig. 2b respectively are multiplied by the antenna pattern in Fig. 3. It is clear that main lobe is directed to the $z > 0$ hemisphere. Minor lobes are significant higher in the Mills array. A color-coded power pattern on a $\theta - \phi$ Cartesian plane in both cases (Mills cross and square array) are shown in Fig. 5a and Fig. 5b respectively. The dark red zone represents the highest power, and the half power level is in the green color (between the yellow and cyan). The analysis of these patterns produces the results presented in Table I, where all data are obtained by numerically analyzing the pattern calculated with a resolution of 1 degree for $\theta$ and $\phi$ . Results indicate that the square array has a higher directivity and a sharper main lobe, but the direction of the main lobe is practically the same.

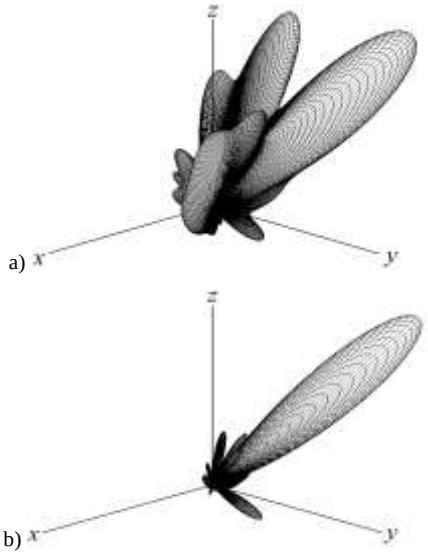


Fig. 4. Field pattern produced by: a) 17 patches Mills cross; b) 81 patches square planar array

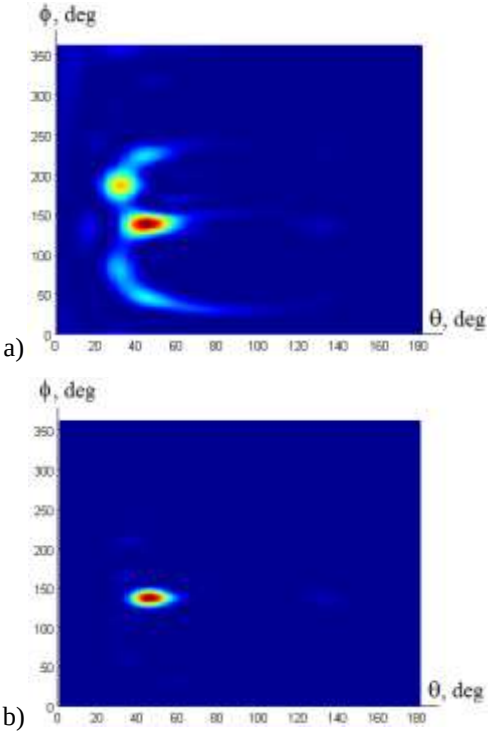


Fig. 5. Normalized power pattern produced by: a) 17 patches Mills cross; b) 81 patches square planar array.

TABLE I. RESULTS OF PATTERN ANALYSIS

| Array | $\theta_0$ deg. | $\phi_0$ deg. | $BW_1$ deg. | $BW_2$ deg. | $D_0$ (dB) |
|---|---|---|---|---|---|
| Mills cross | 43 | 137 | 20 | 30 | 15.5 |
| Square array | 44 | 136 | 16 | 22 | 22.1 |

Note 1- $BW_1$ is the beamwidth on the plane $\phi = \phi_0$ and $BW_2$ is obtained in the perpendicular plane to the plane $\phi = \phi_0$ and crosses the origin.

In order to limit the analysis, in this work were considered square arrays and cross arrays with $M = N = 1, 2, 3$ and $4$ . Thus the number of elements in each array is shown in Table II. Also, the amplitude excitation was limited to a Dolph-Tschebysheff distribution calculated with a side lobe level of 20 dB, resulting in the amplitudes shown in table III, for different values of *M*. It is suitable to note that in a square array, the amplitude of excitation of each antenna is obtained by matrix multiplication of amplitudes vector with its transpose, that is, $\mathbf{A} \cdot \mathbf{A}'$ where $\mathbf{A}$ is a vector formed with the values in table III.

TABLE II. NUMBER OF ANTENNAS IN THE ARRAYS

| *M* | 1 | 2 | 3 | 4 |
|---|---|---|---|---|
| Mills cross | 5 | 9 | 13 | 17 |
| Square array | 9 | 25 | 49 | 81 |

TABLE III. NORMALIZED AMPLITUDES OF EXCITATION OF ELEMENTS OF THE ARRAY ON EACH AXIS.

| *M* | Normalized amplitudes |
|---|---|
| 1 | 1, 0.82, 1 |
| 2 | 0.62, 1, 0.6, 1, 0.62 |
| 3 | 0.59, 0.76, 1, 0.55, 1, 0.76, 0.59 |
| 4 | 0.63, 0.65, 0.85, 1, 0.53, 1, 0.85, 0.65, 0.63 |

In order to evaluate the performance of the array in all its range of operation, a sweep of progressive phase of excitation in both axes with values from -180 degrees to 180 degrees in increments of 20 degrees was carry out. For each case, the pattern was analyzed and parameters of interest were determined.

To study the total coverage of the antenna arrays, in Fig. 6 are shown normalized cumulative power patterns of the square array with 9 antennas (Fig. 6a), 81 antennas (Fig. 6b), and cross array with 5 antennas (Fig. 6c) and 17 antennas (Fig. 6d). In these patterns, the highest power is represented in dark red for the main lobe in each case of progressive phase, that is, the dark red represents the main lobe, although not all main lobes have the same power. It was selected in this way because directivity can be used to analyze the dispersion of power of the array, for different directions of the main lobe. In Fig. 6b and Fig. 6d the spots in dark red indicate that main lobes for these arrays are thinner than those of arrays with power patterns in Fig. 6a and Fig. 6b, this is because these arrays have more antennas, and can produce sharper lobes.

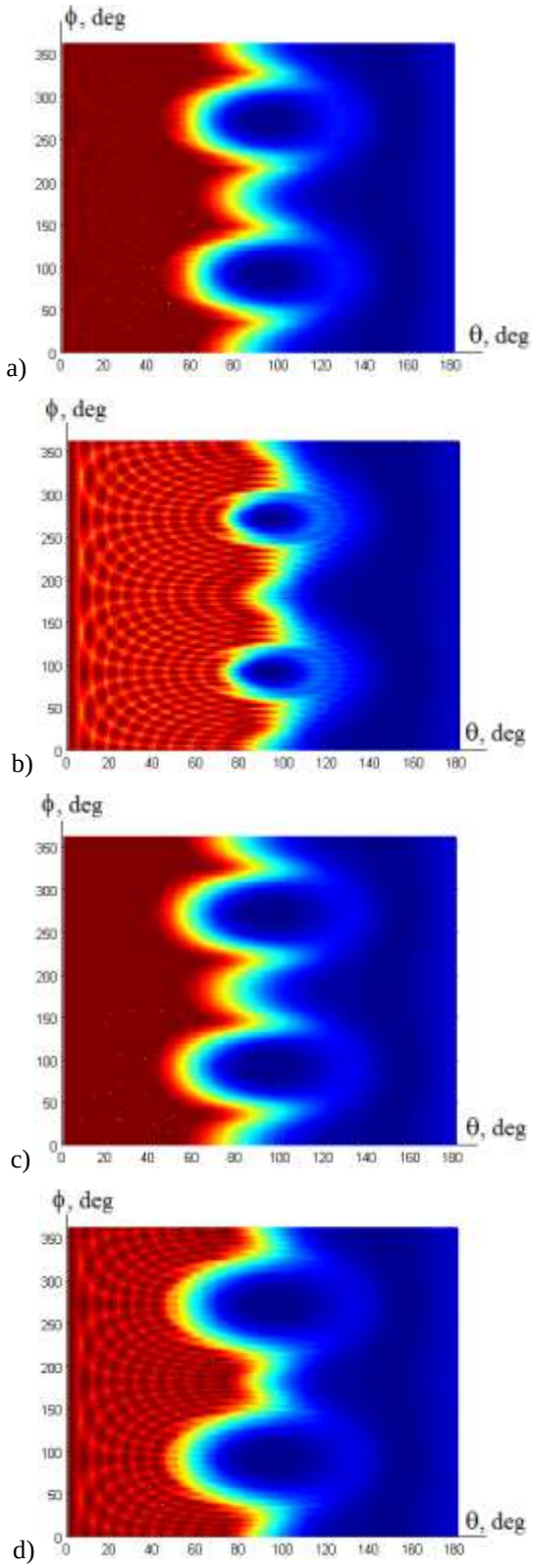


Fig. 6. Normalized cumulative power pattern: a) 9 patches square array; b) 81 patches square array; c) 5 patches cross array; d) 17 patches cross array.

From Fig. 6 it is clear that in no case, the $z > 0$ hemisphere is totally covered. For example, the $\theta = 90°$ and $\phi = 90°$

direction is never reached. However, in the cross array, which is more restricted, it is difficult to reach the $\theta = 60°$ and $\phi = 90°$ direction, while in the square array this direction is covered.

It is convenient to note that, in some cases, two progressive phases can produce a main lobe in the same direction. For example, in the square array with 9 antennas, when $\beta_x = -60°$ and $\beta_y = 0°$, and when $\beta_x = -60°$ and $\beta_y = 180°$ the main lobe is directed to $\theta_0 = 21°$ and $\phi_0 = 0°$, as shown in Fig. 7a and Fig. 7b respectively. The directivity in the first case is 14.4 dB, while in the second case is 11.0 dB. It is clear that a lower directivity indicates the dispersion of energy. In this example, two minor lobes of important amplitude are produced in two other directions.

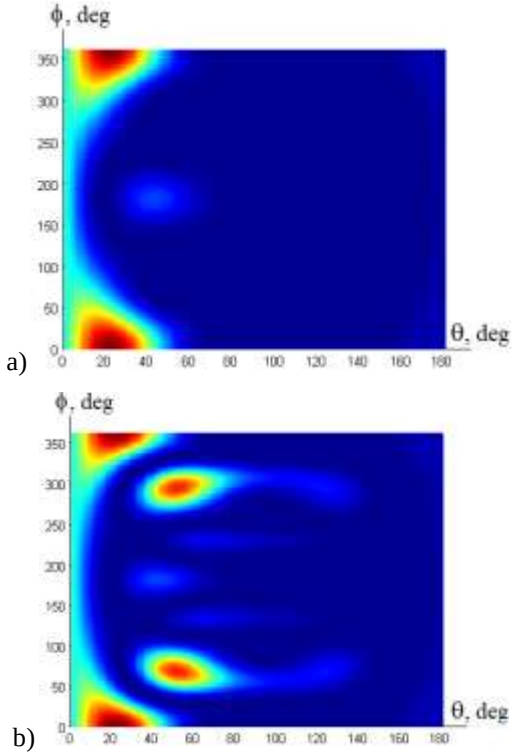


Fig. 7. Normalized power pattern of a 9 patches square array: a) $\beta_x = -60°$ and $\beta_y = 0°$; b) $\beta_x = -60°$ and $\beta_y = 180°$.

Table IV presents the data of cross and square arrays of patches that produce the highest and lowest values of directivity, for the number of elements and excitations considered in this analysis. Based on previous discussion, lower directivity indicates energy dispersion, thus, care should be taken for low directivity cases. If directivity is limited to 0.7 of the highest directivity in each case, the coverage of radiation is reduced as shown in Fig. 8. Comparing Fig. 6b with Fig. 8b for a square array of 81 antennas, it is observed that in the former case it is possible to reach any value of $\phi_0$ up to $\theta_0 \approx 80°$, while in the second case, it is possible to have total azimuthal coverage but limited up to $\theta_0 \approx 50°$. In the cross array case, $\theta_0$ is reduced from 50° to 40° approximately.

TABLE IV. MAXIMUM AND MINIMUM DIRECTIVITY

| Array | $M$ | $\theta_0$ deg. | $\phi_0$ deg. | $BW_1$[1] deg. | $BW_2$[1] deg. | $D_0$ (dB) |
|---|---|---|---|---|---|---|
| Cross | 1 | 71 | 6 | 47 | 58 | 6.7 |
| Cross | 1 | 0 | 45 | 54 | 41 | 11.3 |
| Cross | 2 | 70 | 167 | 26 | 23 | 9.1 |
| Cross | 2 | 13 | 180 | 33 | 31 | 14.2 |
| Cross | 3 | 68 | 339 | 20 | 19 | 10.1 |
| Cross | 3 | 0 | 45 | 25 | 25 | 15.6 |
| Cross | 4 | 57 | 174 | 31 | 33 | 11.0 |
| Cross | 4 | 14 | 180 | 20 | 19 | 16.7 |
| Square | 1 | 72 | 12 | 42 | 39 | 10.1 |
| Square | 1 | 27 | 180 | 36 | 33 | 14.5 |
| Square | 2 | 35 | 65 | 37 | 34 | 11.2 |
| Square | 2 | 34 | 180 | 22 | 20 | 18.3 |
| Square | 3 | 35 | 90 | 32 | 25 | 12.9 |
| Square | 3 | 27 | 180 | 16 | 17 | 21.2 |
| Square | 4 | 63 | 325 | 29 | 29 | 13.8 |
| Square | 4 | 8 | 30 | 12 | 12 | 23.5 |

Note 1- $BW_1$ is the beamwidth on the plane $\phi = \phi_0$ and $BW_2$ is obtained in the perpendicular plane to the plane $\phi = \phi_0$ and crosses the origin.

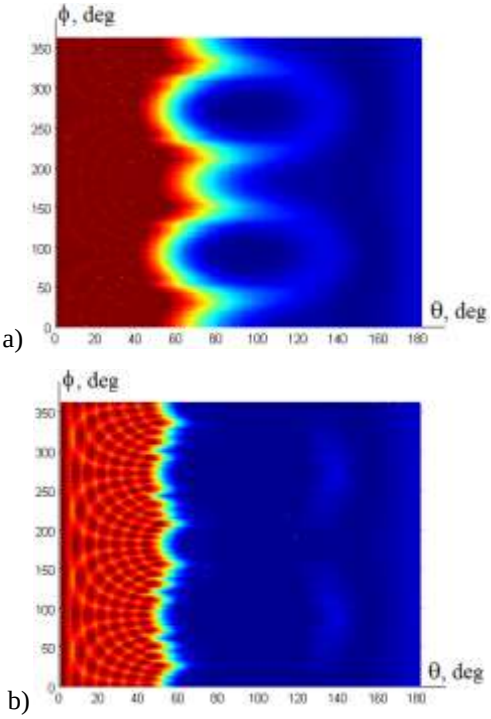

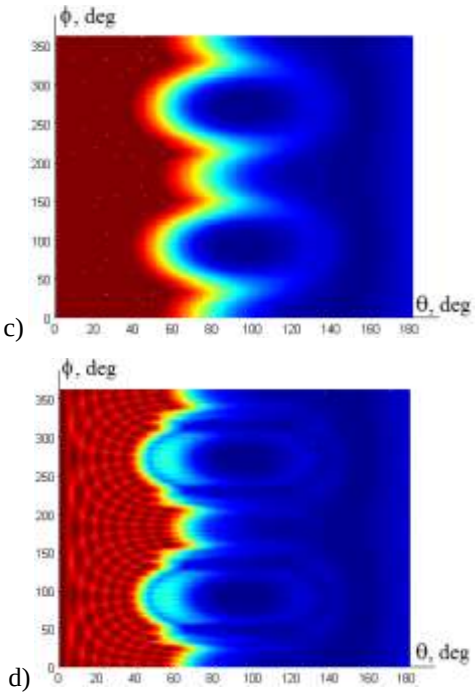


Fig. 8. Normalized cumulative power pattern with directivity grater than 70% of the highest: a) 9 patches square array; b) 81 patches square array; c) 5 patches cross array; d) 17 patches cross array.

## V. CONCLUSION

In this paper an analysis of the Mills cross for 5G mobile handset applications was presented. The main purpose was to determine the radiation coverage for the $z > 0$ hemisphere. To compare its performance, the square planar array with the same amplitude and phase of excitation was used as a reference. In order to obtain realistic results, a rectangular patch antenna was considered in all cases. It was found that Mills cross produces directivities lower than those obtained with the square planar array, and the same happens with the total coverage. However, the number of antennas in the Mills cross is much less than the reference array, thus for cases where directivity of Mills cross of patch antennas is enough to establish a link, this solution will be less expensive.

## REFERENCES

Balanis, Constantine A., (2005). Antenna Theory, Analysis and Design. Wiley-Interscience.

Degel C., F. H. (2014). 3D Sonar System based on Mills Cross Antenna Configuration. Procc. of 2014 Oceans. St. John's, N. L., Canada: IEEE.

Birtill, E. J., (1965). The Application of Phased Arrays to the Analysis of Seismic Body Wave. Series A. Mathematical and Physical Sciences, Phisosophical Transactions of the Roysal Society of London , 421-493.

Groups, Radiocommunication Study. (29 de June de 2016). Recuperado el 11 de August de 2017, de https://www.itu.int/es/ITU-R/Pages/default.aspx

MacPhie R. H., (2007 ). "A Mills Cross Multipicative Array with the Power Pattern of a Convensional Planar Array". IEEE Antennas and Propagation Society International Symposium. Honolulu, Hawaii: IEEE.

Marzetta T. L., (2015). Massive MIMO: An Introduction. Bell Labs Technical Journal .

MacPhie R. H., (2011). "A modified mills cross with elements spaced one wavelength apart". URSI General Assembly and Scientific Symposium. Istambul, Turkey: IEEE.

Mills, B. Y. (1953). A High Resolution Aeriual Systema of a New Type. Australian J. Phys. , 272-278.

Razavi, B. (2009). Design of millimeter-wave CMOS Radios: A Tutorial. IEEE Transactions on Circuits Systems , 4-16.

Recommendation ITU-R. (12 de October de 2015). M.2083-0, M Series Mobile, radiodetermination, amateur and related satellite services. Recuperado el 21 de August de 2017, de https://www.itu.int/es/ITU-R/Pages/default.aspx

Slattery, B. R. (1966). Use of Mills cross receivinf arrays in radar system. Proc. IEE , 1712-1722.

Working Party 5D. (22 de February de 2017). Minimum requirements related to technical performance for IMT-2020 radio interface(s), Document 5/40-E. Recuperado el 30 de May de 2017, de https://www.itu.int/es/ITU-R/Pages/default.aspx

Y. Huo, X. D. (2017). 5G Cellular User Equipment: From Theory to Practial Haerdawre Designs. IEEE , 13992 - 14010.